International Journal of
Automotive Manufacturing and Materials（IJAMM）

Scilight

Article

A Wide-Beam Antenna for Automotive Radar Based on Improved Particle Swarm Algorithm

Bin Wang [1], Zhenhua Li [1], and Shufei Yin [1,2,*]

[1] Shanghai Baolong Automotive Corporation, Shanghai 201619, China
[2] School of Automotive Engineering, Wuhan University of Technology, Wuhan 430070, China
* Correspondence: yinshufei@chinabaolong.net
Received: 26 August 2024; Revised: 09 September 2024; Accepted: 11 September 2024; Published: 23 September 2024

Abstract: The traditional automotive corner radar antenna has the problem that the horizontal filled of view (FOV) is not large enough, which affects wide detection area capability and driving safety. In order to solve the problem, this paper proposes a wide-beam antenna design method for automotive corner radar based on improved particle swarm optimization (IPSO) algorithm. The mathematical model of comb-line antenna for 77 GHz corner radar is established and combined with the IPSO algorithm to achieve wide beam. The algorithm avoids the search process falling into local optimum by introducing an adaptive shrinkage factor and chaotic disturbance when the non-superior particle position is updated. The computational results show that the convergence of the IPSO algorithm is significantly better than standard particle swarm optimization (SPSO) in wide beam forming under the same number of iterations.

Keywords: automotive corner radar; particle swarm optimization (PSO); comb-line antenna; beamwidth; wide-beam antenna

1. Introduction

In recent years, with the rapid development of the automotive industry, the improvement of vehicle safety performance has become an increasingly important issue. In vehicle safety systems, radar technology is widely used, of which corner radar is a common and critical sensor. Corner radar can detect the position and speed of objects in surrounding environment by sending and receiving electromagnetic wave, thus helping drivers to warn and avoid potential collision risks in time. As an important part of the millimeter wave radar system, antenna specifications affect critical performance of the radar, such as detection range, filled of view (FOV), and angular resolution. By improving the performance of antenna, the detection capability of the radar will also be improved. Automotive radar with different applications has different requirements on antenna gain and beamwidth [1–7]. For applications of short and medium range radars such as blind spot detection, lateral lane collision warning, lane change assistance, antennas with a large FOV to detect the target in a wide range is essential. FOV and blind zone of the corner radar is shown in Figure 1.

When automotive corner radar is used for lateral and rear range and angle measurement, it can be used to detect moving targets within a short range, which requires the antenna with a wide beam. This wide area detection can largely avoid traffic accidents. Usually, radar FOV requires the antenna to achieve a coverage of 6 dB horizontal beamwidth of 150°. However, the 6 dB beamwidth for the most radar antennas is generally less than 120° [8–11], which is poor performance for the detection of large FOV in the lateral and rear directions, and there are problems such as blind areas and insufficient detection range. Meanwhile, the vehicle radar antenna requires low cost, low profile and high integration characteristics.

Microstrip antenna, waveguide slot antenna and lens antenna are commonly used for automotive radar. In [12], a series-fed microstrip patch antenna array can realize the side lobe level (SLL) of −22 dB with half power beamwidth of 10 degree. In [13], antenna array with two columns shows the simulation gain of

17.2 dBi, SLL of 12.9 dB, and HPBW of 5.7°. In [14], a design of comb-line patch array with low side lobe level for automotive collision avoidance radar at 77 GHz is discussed and simulation results show that SLL of array is better than −21 dB and the final antenna gain is around 24.7 dBi. A single beam offset parabolic reflector antenna for a highly integrated module is designed [15]. In [16], a structure of the antenna, composed of three types of horn, lens, and prism antennas with different directivities, produces a radiation pattern that had both a narrow FOV at a long-range detection and wide FOV at short range detection. Different types of horn antennas for use in automotive radar are proposed, but these antennas are characterized by a larger footprint, high gain, and narrower beam [17−20]. A lens antenna for a wide scan angle of ±85° in azimuth plane has a maximum antenna gain of 15 dBi at 82.5 GHz and gain drop of less than 2.75 dB for the edge feeds [21]. In [22], the antenna with wide bandwidth is designed, but the beam width is not enhanced. Ina two-layer broadband wide-beam microstrip antenna for 79 GHz automotive radar is proposed, which consists of microstrip lines, radiating patches and parasitic patches, to achieve low SLL of −19 dB at E-plane and −17 dB at H-plane, respectively. In [22], a substrate integrated waveguide (SIW) based broadband millimeter-wave slot array antenna is proposed for 79 GHz automotive radar applications. The simulated 10 dB impedance bandwidth of the designed antenna is from 75.6 to 81.4 GHz and the realized gain is 10.5–12 dB within 76–81 GHZ frequency band.

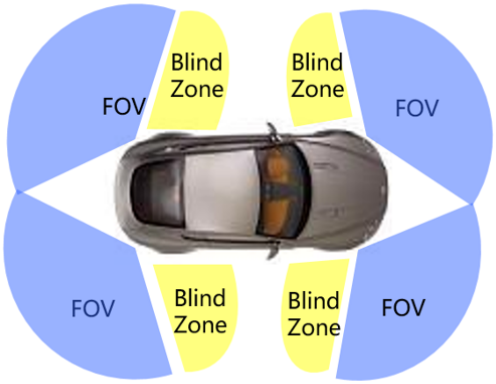

Figure 1. FOV of corner radar.

There are not many references on the wide-beam performance of vehicle radar antennas, especially in the 77 GHz. In [23−29], low-band antennas with wide-beam are proposed. In [23], the concept of a self-mixed antenna array operating at 34–39 GHz was proposed to obtain a wide beam coverage with the required gain. However, the high gain is obtained by increasing the spacing between the elements and using devices such as amplifiers, so the antenna system is complex and not applicable to vehicle mounted radar with wide-beam antennas. In [24], the authors proposed a dual-polarized antenna consisting of four differentially fed patches, four short-circuited vias and a square metal cavity. The beamwidth measured in the E-plane is greater than 116°. a multi-resonant patch antenna fed by a coupling slot is explored in [27]. The beamwidth of this structure can reach 125°. An SIW-based slot antenna was proposed in [28]. By integrating the structures of magnetic and electric dipoles, a wide beamwidth of 140° was observed in both E- and H-planes. In [29], a 24-GHz horizontally-polarized 1 × 8 patch antenna array is developed for automotive radar applications and exhibits a wide beamwidth of 150° and a high gain of 11.1 dBi. However, for the 77 GHz frequency band, the addition of parasitic patches between adjacent patches will be a technical problem, due to the limited spacing and the enhancement of coupling effect. In [30], a planar array with wide main-beam scanning range is proposed. The measured results show that it is able to scan its main beam from −75° to +75° in both xoz- and yoz-planes. In [31], a SIW probe coupling method was proposed to widen the beamwidth, but the feed net is complex and occupies a large area, which is difficult to meet the small size requirement of automotive radar. A sector beam transmitting antenna for 79 GHz automotive short range radar (SRR) applications was proposed in [32]. The antenna has three channels with different beam directions to cover a wide

detection area.

In order to overcome the limitations of the horizontal FOV is not large enough, this paper proposes a new wide beam antenna design method. Because the optimization of antenna is a highly nonlinear problem, there are commercial electromagnetic simulation software such as ANSYS, CST can do electromagnetic simulation optimization, but the time of electromagnetic simulation of antenna array is so long. It is difficult to optimize the impedance matching characteristics and gain pattern of the antenna array, so necessary to use optimization algorithms. The application of intelligent algorithms [33–37] has achieved good results.

Particle swarm optimization (PSO) algorithm is an adaptive global optimization heuristic algorithm, which originated from the study of the movement behavior of groups of organisms such as flocks of birds and schools of fish. Through more than decade development, PSO has been widely used in neural network training, fuzzy system control, electromagnetic engineering and array synthesis. Although similar to genetic algorithm, both are stochastic optimization algorithms, but in comparison, PSO is more simple, easy to implement, fast search speed, and contains fewer parameters, so it has received wide attention. The standard PSO, like other algorithms, suffers from the problems of low search range and easy convergence to local optimum. Therefore, various improvement algorithms, such as inertia factor, shrinkage factor, and hybrid particle swarm algorithm, have been developed to improve the convergence accuracy and search success rate of the algorithm.

In this paper, we use an improved particle swarm optimization (IPSO) algorithm with chaotic disturbance of the non-superior particles update to avoid the search falling into local optimum. Adaptive shrinkage factor and fitness function weighting factor are used to optimize characteristics of traditional comb-line antenna. A wide beam is achieved to verify the efficient feasibility of this method. At boresight, the gain obtained by IPSO algorithm is increased 2.5 dB and the horizontal FOV of 6 dB beam width is increased 20°. In order to compare with the FOV of traditional antenna, rectangular series-fed antenna and comb-line antenna with the same length are simulated respectively. The horizontal FOV of comb-line antenna is 162°, which is larger than previous antenna beamwidth of 102° and 109°. The gain is increased 3 dB at ±45° of antenna pattern, which is used to improve the radar detection performance in rear cross traffic alert (RCTA) and rear collision warning (RCW). Especially at ±75°, the gain is increased nearly 8 dB, which has a greater improvement on the blind spot detection (BSD) and helps driver to improve the driving safety.

2. Antenna Design

Microstrip antennas are widely used by vehicle radar manufacturers due to their simple structure, light weight, easy integration and suitable for mass production. Compared to series-fed patch antenna [38–40], the microstrip comb-line array antenna has the advantages of wider beam, smaller occupied area and easy to achieve lower SLL. There are two types of the comb-line array, traveling wave array and standing wave array. Traveling wave array is loaded with matched load at the terminal, the spacing between elements need not be equal to half of the wave length $\lambda_e/2$, the power is radiated by each comb element and finally consumed in the load. Standing wave array is open circuit at the terminal, the spacing between elements should be equal to $\lambda_e/2$. The antenna designed in this section is a standing wave antenna, and the specifications of the antenna are as follows:

(1) Center frequency at 76.5 GHz

(2) Antenna gain ⩾ 11 dB

(3) SLL < −17 dB

(4) Bandwidth > 1 GHz (S11 < −10 dB)

(5) FOV (6 dB beam width in azimuth) > 150°

The structure diagram of comb-line array is shown in Figure 2, with the number of element N = 10, width W_i, length L_i, spacing d_i and feed line width b. The antenna is printed on the Rogers RO3003 s($\varepsilon_r = 3$, $tan\delta = 0.001$) with a thickness of 0.127 mm.

The array with Taylor amplitude taper shows a radiation pattern whose first several sidelobes close to the main beam are at the same level while the rest of lobes decay monotonically. The weighted distribution (unit voltage), is expressed as $I1{:}I2{:}I3{:}I4{:}I5{:}I6{:}I7{:}I8{:}I9{:}I10 = 0.29{:}0.39{:}0.59{:}0.83{:}1{:}1{:}0.83{:}0.59{:}0.39{:}0.29$, with an SLL of −20 dB, which is presented in Equation (1) [10].

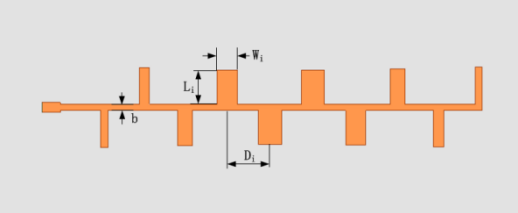

Figure 2. Structure diagram of comb-line array.

$$[V]=[Z_i][I_i]=I \tag{1}$$

Z_i is the normalized characteristic impedance of each comb to the main feeder, and I is the unit matrix, so the above equation can be converted to

$$[V][I_i]^{-1}=[Z_i][I_i][I_i]^{-1} \tag{2}$$

$$[Z_i]=[I_i]^{-1} \tag{3}$$

The width of each comb W_i can be calculated by the following equation.

When $Z_i<(44-2\varepsilon_r)\Omega$, there are:

$$\frac{W_i}{h}=\frac{2}{\pi}\left\{R-1-\ln(2R-1)+\frac{\varepsilon_r-1}{2\varepsilon_r\left[\ln(R-1)+0.293-\frac{0.517}{\varepsilon_r}\right]}\right\} \tag{4}$$

$$R=\frac{377\pi}{2Z_i\sqrt{\varepsilon_r}} \tag{5}$$

ε_r is effective dielectric constant.

When $Z_i\geq(44-2\varepsilon_r)\Omega$, there are:

$$\frac{W_i}{h}=\frac{8e^H}{e^{2H}-2} \tag{6}$$

$$H=\frac{Z_i\sqrt{2(\varepsilon_r+1)}}{120}+\frac{\varepsilon_r-1}{\varepsilon_r+1}\left(0.2258+\frac{0.1208}{\varepsilon_r}\right) \tag{7}$$

Using the above equation, it calculates the width of the element corresponding to the excitation distribution, and calculates the length of the element L_i by the following equation.

Each comb is a T-joint at the feed and the T-joint effect needs to be taken into account. The length L_i can be calculated by the following equation

$$L_i=\frac{\lambda_{ei}}{2}-\Delta l_i-(\frac{b}{2}-n_i) \tag{8}$$

The empirical equation of Δl_i is as follows:

$$\Delta l_i=0.412h\left(\frac{\varepsilon_r+0.3}{\varepsilon_r-0.258}\right)\left(\frac{\frac{W_i}{h}+0.264}{\frac{W_i}{h}+0.8}\right) \tag{9}$$

λ_{ei} is the equivalent waveguide wavelength of each comb, and Δl_i can be calculated from Equation (9). b is the width of the main feed line, and n_i is the correction factor determined from Equation (10).

$$n_i=d\left\{0.5-0.16\left[1+\left(\frac{2d}{\lambda_e}\right)^2-2\ln\left(\frac{Z_b}{Z_{wi}}\right)\frac{Z_b}{Z_{wi}}\right]\right\} \tag{10}$$

$$d = \frac{120\pi h}{Z_b\sqrt{\varepsilon_r}} \tag{11}$$

In Equation (10), Z_b is the impedance of feed line with width b and Z_{wi} is the impedance of comb.

3. Improved Particle Swarm (PSO) Algorithm

3.1. Standard PSO Algorithm

In PSO algorithm, the solution of each optimization problem is considered as a bird (i.e., particle) in search space. All particles have an adaptation value determined by the optimized function and a speed that determines the direction and rate of their flight. The particles follow the current optimal particle in the solution space. The algorithm initializes a group of random particles and then finds the optimal solution by iteration. In each iteration, the particles update their velocity and position by tracking two "extremes", i.e., the individual extremes and the global extremes. In the N-dimensional target search space, a particle swarm is composed of particles with population n. The position of the i particle in the j dimension is X_{ij}, its velocity is V_{ij}, the current optimal position of the particle is $pbest_{ij}$, and the current optimal position of the whole swarm is $gbest_j$. For the kth iteration, the velocity and position are updated as follows.

$$V_{ij}^{k+1} = \omega V_{ij}^{k+1} + c_1 r_1 (pbest_{ij} - X_{ij}^k) + c_2 r_2 (gbest_j - X_{ij}^k) \tag{12}$$

$$X_{ij}^{k+1} = X_{ij}^k + V_{ij}^{k+1} \tag{13}$$

where ω is the inertia factor, c_1 and c_2 are acceleration factors, and r_1 and r_2 are random numbers uniformly distributed between [0~1].

3.2. Adaptive Inertia Factor

In order to improve the global search capability of the PSO algorithm, a nonlinear dynamic inertia factor ω is used, whose expression is as follows:

$$\omega = \begin{cases} \omega_{\min} - \dfrac{(\omega_{\max} - \omega_{\min})(f - f_{\min})}{(f_{avg} - f_{\min})} & ,f \le f_{avg} \\ \omega_{\max} & ,f \ge f_{avg} \end{cases} \tag{14}$$

where ω_{max}, ω_{min} denote the maximum and minimum values of ω, respectively, f denotes the current objective function value of the particle, and f_{avg} and f_{min} denote the average and minimum objective values of all the current particles, respectively. In the above equation, the inertia factor adaptively changes with the target function value of the particle.

When the objective value of each particle tends to be the same or tends to be locally optimal, it will increase the value of inertia weight. When the objective value of each particle is more dispersed, it will decrease the value of inertia weight. For the particle whose objective function is better than the average objective value, the corresponding inertia weight factor is smaller in order to protect the particle. Conversely for the particle whose objective function value is worse than the average objective value, the corresponding inertia weight factor is larger, making the particle move towards closer to the better search area.

3.3. Adaptation Function Weighting Factor

The mathematical model for fitness function of the particles can be described by the following equation.

$$\begin{aligned} &\min f = f(X) \\ &= \begin{cases} \beta \cdot \sum_{m=1}^{M} \max(\left| F(X,\theta_m) \right| - \left| AF(\theta_m) \right|, 0)^2 + S11, \theta_1 \le \theta \le \theta_2 \\ \sum_{m=1}^{M} \max(\left| F(X,\theta_m) \right| - \left| AF(\theta_m) \right|, 0)^2 + S11, \theta < \theta_1 \quad or \quad \theta > \theta_2 \end{cases} \end{aligned} \tag{15}$$

where: $X = (x1, x2, ..., xN)$, M denotes the number of angular sampling points defined in the formula; θ_m is the m th sampled angular, $F(X, \theta_m)$ is the optimal radiation pattern obtained from the simulation software,

$AF(\theta_m)$ is the target radiation pattern, $S11$ denotes the return loss of the antenna array at 76.5 GHz frequency extracted from the simulation software, β is the weighting factor of the fitness function, which can adjust the convergence speed of the particle swarm in the region from θ_1 to θ_2. Because the wide beam performance is more difficult to achieve, fitness function can more easily obtain a smaller value of $S11$, it can avoid problem that the $S11$ value is small, while difference of antenna pattern is large.

3.4. Chaotic Disturbance

Chaos is a common phenomenon in nonlinear systems, which is characterized by ergodicity and intrinsic randomness, and can traverse all states without repetition in a certain range according to its own laws.

The logistic chaos mapping relationship is as follows:

$$y_{i+1} = \mu y_i (1 - y_i) \tag{16}$$

where $y \in (0, 1)$, $\mu \in (2, 4]$, and when $\mu = 4$, the mapping is completely in a chaotic state, when the chaotic sequence of (0, 1) is generated with better ergodicity. The introduction of chaotic disturbance in PSO can improve the quality of the initial particles and make the initial particle distribution more uniform. The chaotic disturbance of the positions of non-superior particles in each iteration effectively avoids algorithm falling into local optimality too long to jump out, which improves the convergence speed very well.

Chaotic variation is applied to some non-superior particles with poor adaptation, and their chaotic disturbance positions are updated as

$$X_{ij}^{k+1} = X_{ij}^{k} + \eta(2y_{ij} - 1) \tag{17}$$

where: η is the radius of the chaotic search region, y_{ij} is calculated from Equation (15).

In summary, the IPSO algorithm is implemented as follows:

Step 1: initialize the velocity and position of the particle according to Equations (12) to (14);

Step 2: introduction of weighting factors to calculate the fitness of the particles;

Step 3: Chaotic disturbance of non-superior particles according to Equation (17) and obtaining new positions;

Step 4: update the individual optimum *pbest* of each particle and the global optimum *gbest* of the population;

Step 5: If the convergence condition is satisfied, the operation terminates, otherwise skip to the second step.

4. Optimization Results

In this paper, we add branches to the traditional comb-line antenna and increase the beam width by beamforming, because the corner radar is usually installed at an angle of 45° to the body of car, and the rearward and lateral directions are related to the detection range of RCTA and RCW, so the target gain pattern at ±45° is improved as shown in Figure 3.

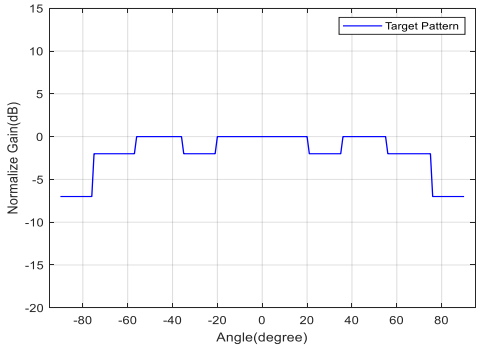

Figure 3. E Plane of Target Pattern.

As shown in Figure 4, the size of comb and spacing between elements will affect the radiation pattern and the standing wave matching for comb-line antenna. In order to reduce the optimization time and design complexity, the size of antenna elements according to the theoretical Equations (4), (6), (8) is calculated. Because the excitation of the comb-line array has been determined, so the width of the comb will not be changed. The length and the spacing of the comb need to be optimized. The phase error of series feed is easy to accumulate gradually among the array elements, eventually accumulating a large deviation. Due to the phase error caused by the shortening effect of the microstrip boundary and the accumulation of offsets, a distribution of unequally spaced line array is used to ensure that each element is distributed in the same phase. Total number of 29 parameters need to be optimized in the algorithm for D_i, L_i, Ls_i and Ws_i. Because the excitation of antenna array is symmetrically distributed using Taylor weighting and D_i, L_i also use symmetric length, only L_0~L_4 D_0~D_4 need to be optimized. In order to further reduce the variables, Ls_i can be counted as a single variable, so that the total number of optimized parameters is reduced to 16. The range of values for each parameter of the antenna significantly affects the convergence time and the convergence results. The range of values for D is set to [1.29 mm, 1.40 mm], for L set to [1.10 mm, 1.20 mm], for *Ls* set to [1.10 mm, 1.20 mm], and for *Ws* set to [0.23 mm, 0.45 mm].

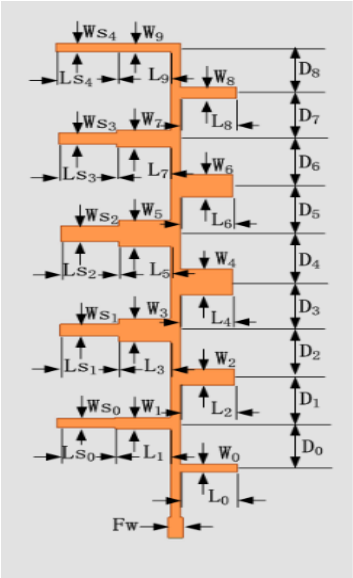

Figure 4. Structure diagram of beamforming comb-line array.

The optimization algorithm is executed in Matlab software, and the macro command Ansys-Matlab-API is used to control the electromagnetic simulation software Ansys through the Matlab program to automatically complete the antenna modeling, simulation and other operations. The results are brought into the optimization program written in Matlab for optimization. The values of the antenna parameters obtained after optimization are listed in Table 1.

A Low SLL in the elevation plane and wide beam in the horizontal plane are presented through the optimized branches. In Figure 5a, the simulation result of −10 dB bandwidth is 1.9 GHz (75.5~77.4 GHz). Figure 5b shows the E-plane and H-plane radiation pattern of the modified comb-line antenna, and the simulation result of the SLL is −19 dB, which meets the requirement of automotive radar. The maximum gain of the antenna at 77 GHz is 12 dBi, the boresight gain is 10.9 dB, the azimuthal FOV of 6 dB beamwidth is 162°, and the elevation FOV of 6 dB beamwidth is 24°. Figure 6 shows the comparison between the target pattern and the optimized radiation pattern, which shows that the gain difference within ±75° FOV is less than 2 dB.

Table 1. Values of the Design Parameters of comb-line antenna.

Parameter	Value (mm)	Parameter	Value (mm)
W_0	0.23	L_5	1.10
W_1	0.32	L_6	1.11
W_2	0.48	L_7	1.14
W_3	0.65	L_8	1.18
W_4	0.75	L_9	1.20
W_5	0.75	Ls_0	1.22
W_6	0.65	Ls_1	1.22
W_7	0.48	Ls_2	1.22
W_8	0.32	Ls_3	1.22
W_9	0.23	Ls_4	1.22
Ws_0	0.26	D_0	1.29
Ws_1	0.32	D_1	1.32
Ws_2	0.41	D_2	1.36
Ws_3	0.3	D_3	1.38
Ws_4	0.23	D_4	1.39
L_0	1.20	D_5	1.38
L_1	1.18	D_6	1.36
L_2	1.14	D_7	1.32
L_3	1.11	D_8	1.29
L_4	1.10	Fw	0.31

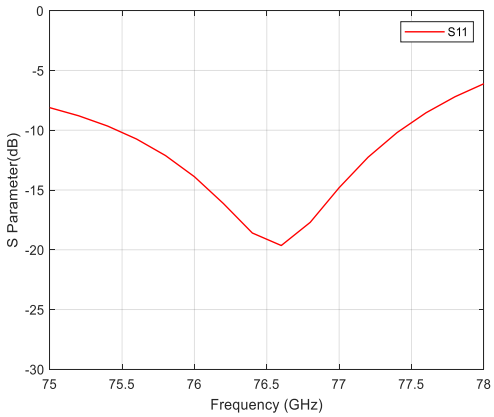

(a) Reflection coefficient magnitude;.

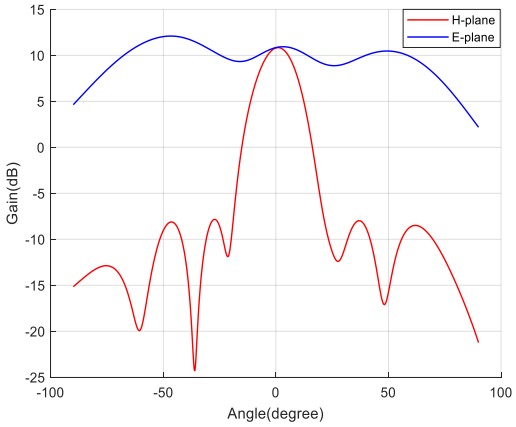

(b) Gain pattern in principal radiation planes.

Figure 5. Simulation results of beamforming comb-line array.

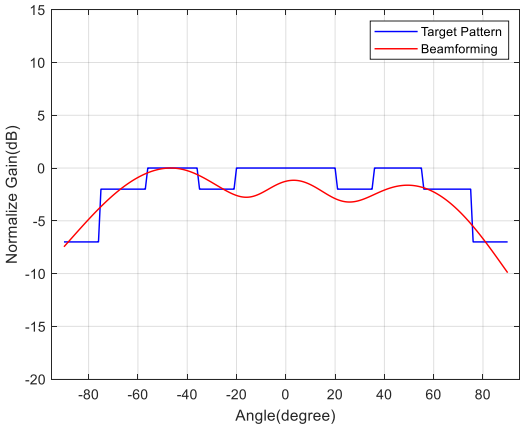

Figure 6. Comparison of target pattern and beamforming pattern.

In order to compare with FOV of traditional corner radar antenna, the rectangular series-fed antenna with the same length in Figure 7 and the comb-line microstrip antenna in Figure 2 are simulated.

Figure 7. Structure diagram of Series-fed antenna array.

In Figure 8, the horizontal beam width of the comb-line antenna array is wider than series-fed antenna array. The horizontal FOV of the beamforming comb-line antenna array proposed in this paper is 60° larger than these two traditional vehicle-mounted radar antennas, and the gain is enhanced 3 dB at ±45°, which is used to improve the detection performance of RCTA and RCW, especially at a large angle ±75°, the gain is enhanced by nearly 8 dB. The performance of BSD could be greatly improved.

Figure 9 shows the comparison of horizontal beamwidths between improved PSO and standard PSO. The convergence result of IPSO is significantly better than the standard particle swarm optimization (SPSO) under the same number of iterations. The gain of SPSO is 2.5 dB lower compared with the IPSO at boresight

and beam width is narrower 20°.

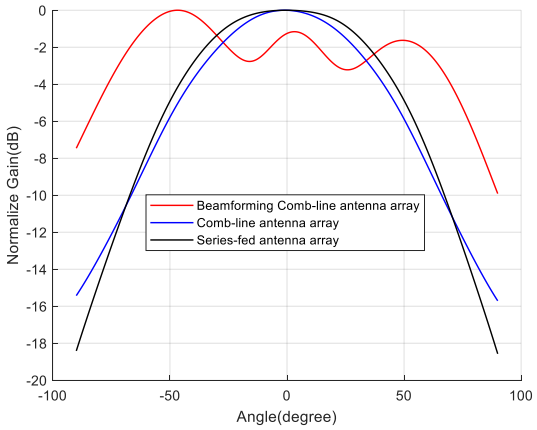

Figure 8. Horizontal beamwidths of different antennas.

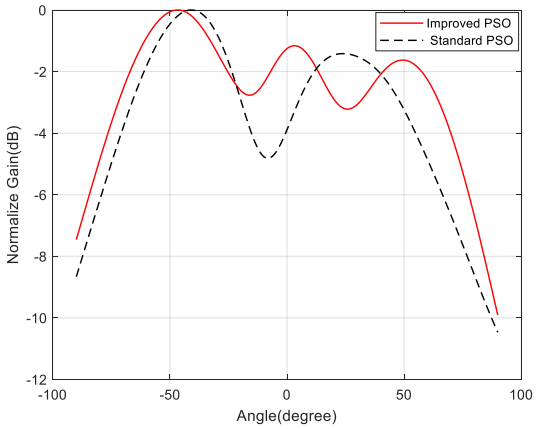

Figure 9. Comparison of horizontal beamwidths between improved PSO and standard PSO.

5. Conclusions

In this paper, a wide-beam antenna design method for automotive corner radar is proposed to improve performance of BSD and RCW. By adding branches to the conventional comb-line antenna and adopting an IPSO algorithm with adaptive inertia factor and chaotic disturbance, it is successfully used for beamforming on radiation pattern of array antenna. SLL of the comb-line antenna on the H-plane is 19 dB and the gain at 45° area is enhanced 3 dB. FOV of 162° and a gain of 10.9 dB are observed at 77 GHz. Especially the corner radar is usually installed at a 45° angle to the body of the car, the gain of antenna has poor performance in large FOV, after beamforming the gain enhanced 8 dB at ±75° compared with the traditional automotive radar antenna.

Author Contributions: Conceptualization, B.W. and Z.L.; methodology, B.W. and S.Y.; software and validation, Z.L.; formal analysis, B.W.; investigation, S.Y.; resources, S.Y.; data curation, S.Y.; writing—original draft preparation, B.W. and S.Y.; writing—review and editing, B.W. and Z.L.; visualization, B.W. and Z.L. All authors have read and agreed to the published version of the manuscript.

Funding: This research is funded by Ministry of Industry and Information Technology of China-Software Development and Application Project of Model-based Systems Engineering.

Institutional Review Board Statement: Not applicable.

Informed Consent Statement: Not applicable.

Data Availability: Statement: Not applicable.

Acknowledgments: The author would like to thank Shanghai Baolong Automotive corporation.

Conflicts of Interest: The authors declare no conflict of interest.

References

1. Mukherjee A.; Sarkar D. Compact MIMO Radar of Improved Angular Resolution Using Interleaved Array Geometry. *IEEE Trans. Veh. Technol.* **2024**, *73*, 6158–6170.
2. Pirkani; Norouzian, F.; Cherniakov, M.; Gashinova, M. Adaptive Digital Beamforming for Radar Interference Mitigation. In Proceedings of the 2024 International Radar Symposium (IRS), Wroclaw, Poland, 2 – 4 July 2024; pp. 12–17.
3. Chen, H.; Zhang, X.; Shen, Y.; Shen, L. A Study of Performance Assessment in Automotive Millimeter Wave Radar Industry. In Proceedings of the 2024 Photonics & Electromagnetics Research Symposium (PIERS), Chengdu, China, 20 January 2024; pp. 1–9.
4. Ren Q.; Bencivenni C.; Carluccio G.; Shivamurthy H. T.; De Graauw A.; Jansen F.; Zaman A. U. Gapwaveguide Automotive Imaging Radar Antenna with Launcher in Package Technology. *IEEE Access* **2023**, *11*, 37483–37493.
5. Zang Z.; Zaman A. U.; Yang J. Single Layer Dual Circularly Polarized Antenna Array Based on Ridge Gap Waveguide for 77 GHz Automotive Radar. *IEEE Trans. Antennas Propag.* **2022**, *70*, 5977–5982.
6. *F*ang, C.; Su, M.; Liu, Y. A Low Side Lobe Level Microstrip Antenna Array for 77 GHz Automotive Radar. In Proceedings of the 2020 IEEE 6th International Conference on Computer and Communications (ICCC), Chengdu, China, 11–14 December 2020; pp. 448–452.
7. Xu J.; Hong W.; Zhang H.; Wang G.; Yu Y.; Jiang Z.H. An Array Antenna for Both Long- and Medium-Range 77 GHz Automotive Radar Applications. *IEEE Trans. Antennas Propag.* **2017**, *65*, 7207–7216.
8. Zhang W.; Li N.; Zheng Z.; Shi L.; Li Z.; Yu J.; Kasper E. Passive and Active Verification of Serial-Fed Patch Antenna Array for 77 GHz Automotive Corner Radar. In Proceedings of the 2020 IEEE MTT-S International Wireless Symposium (IWS), Shanghai, China, 20–23 September 2020; pp. 1–3.
9. Yu Y.; Hong W.; Zhang H.; Xu J.; Jiang Z.H. Optimization and Implementation of SIW Slot Array for Both Medium- and Long-Range 77 GHz Automotive Radar Application. *IEEE Trans. Antennas Propag.* **2018**, *66*, 3769–3774.
10. Pazare, N.; Kamble, V. A 77 GHz Microstrip Comb-Line Antenna Array for Automotive RADAR application. In Proceedings of the 2022 Antenna Measurement Techniques Association Symposium (AMTA), Denver, CO, USA, 9–14 October2022; pp. 1–5.
11. Hamberger G. F.; Spath S.; Siart U.; Eibert T. F. A mixed circular/linear dual-polarized phased array concept for automotive radar-planar antenna designs and system evaluation at 78 GHz. *IEEE Trans.* **2019**, *67*, 1562–1572.
12. Jian, B.; Yuan, J.; Liu, Q. Procedure to Design a Series-fed Microstrip Patch Antenna Array for 77 GHz Automotive Radar. In Proceedings of the 2019 Cross Strait Quad- Regional Radio Science and Wireless Technology Conference (CSQRWC), Taiyuan, China, 18–21 July 2019; pp. 1–2.
13. Yoo S.; Milyakh Y.; Kim H.; Hong C.; Choo H. Patch Array Antenna Using a Dual Coupled Feeding Structure for 79 GHz Automotive Radar Applications. *IEEE Antennas Wirel. Propag. Lett.* **2020**, *19*, 676–679.
14. Yasini, S.; Mohammadpour-Aghdam, K. Design and simulation of a Comb-line fed microstrip antenna array with low side lobe level at 77 GHz for automotive collision avoidance radar. In Proceedings of the 2016 Fourth International Conference on Millimeter-Wave and Terahertz Technologies (MMWaTT), Tehran, 20 – 22 December 2016; pp. 87–90.
15. Park, D. -H. Design and Analysis of Single Beam Parabolic Reflector Antenna in LTCC for Millimeter Wave Automotive Radar. In Proceedings of the 2019 IEEE International Conference on Microwaves, Antennas, Communications and Electronic Systems (COMCAS), Tel-Aviv, Israel, 4–6 November 2019; pp. 1–3.
16. Nagaishi, H.; Kuriyama, A.; Kuroda, H.; Kitayama, A. Horn and Prism Antenna for Dual Range and Dual FOV Automotive Radar Using **77**-GHz Band. In Proceedings of the 2018 18th International Symposium on Antenna Technology and Applied Electromagnetics (ANTEM), Waterloo, ON, Canada, 19–22 August 2018; pp. 1–2.
17. Kuriyama, A.; Nagaishi, H.; Kuroda, H.; Takano, K. A high efficiency antenna with horn and lens for 77 GHz automotive long range radar. In Proceedings of the 2016 European Radar Conference (EuRAD), London, UK, 5 – 7 October 2016; pp. 378–381.
18. Garcia-Tejero A.; Burgos-Garcia M.; Merli F. High-Efficiency Injection-Molded Waveguide Horn Antenna Array for 76–81 GHz Automotive Radar Applications. In Proceedings of the 2022 19th European Radar Conference (EuRAD), Milan, Italy, 28–30 September 2022.
19. Ranade S.R.; Nair D.U. Design of a substrate integrated waveguide H plane Horn antenna on a PTFE substrate for automotive radar application. In Proceedings of the 2011 IEEE Applied Electromagnetics Conference (AEMC), Kolkata, India, 18–*22* December 2011.
20. Kumar, A.; Srivastava, S. High Gain Three Dimensional SIW Horn Antenna Array for Automotive Radar Applications. In Proceedings of the 2018 IEEE MTT-S International Microwave and RF Conference (IMaRC), Kolkata, India, 28–30 November 2018; pp. 1–4.
21. Saleem M.K.; Vettikaladi H.; Alkanhal M.A.S.; Himdi M. Lens Antenna for Wide Angle Beam Scanning at 79 GHz for Automotive Short Range Radar Applications. *IEEE Trans. Antennas Propag.* **2017**, *65*, 2041–2046.

22. Liu, Y.; Bai, G.; Yagoub, M. C. E. A 79 GHz Series Fed Microstrip Patch Antenna Array with Bandwidth Enhancement and Sidelobe Suppression. In Proceedings of the 2020 International Conference on Radar, Antenna, Microwave, Electronics, and Telecommunications (ICRAMET), Tangerang, Indonesia, 18 – 20 November 2020; pp. 155–158.
23. Shi, M.; Wu, Q.; Yu, C.; Wang, H.; Hong, W. Broadband Center-Fed SIW Slot Array Antenna with Multi-Layer Transition for 79 GHz Automotive Radar. In Proceedings of the 2019 International Symposium on Antennas and Propagation (ISAP), Xi'an, China, 27–30 October 2019; pp. 1–3.
24. Kornprobst J.; Mittermaier T. J.; Eibert T. F. A Millimeter-Wave Self-Mixing Array with Large Gain and Wide Angular Receiving Range. *IEEE Trans. Antennas Propag.* **2018**, *66*, 702–711.
25. Sun, J.; Zhang, X.; Leyao, W. A Groove Gap Waveguide Antenna System for **77**GHz Automotive Radar Applications. In Proceedings of the 2023 IEEE 11th Asia-Pacific Conference on Antennas and Propagation (APCAP), Guangzhou, China, 15 July 2023; pp. 1–2.
26. Chen X.; Qin P.-Y.; Guo Y.J.; Fu G. Low-profile and wide beamwidth dual-polarized distributed microstrip antenna. *IEEE Access* **2017**, *5*, 2272–2280.
27. Kornprobst J.; Wang K.; Hamberger G.; Eibert T. F. A mm-wave patch antenna with broad bandwidth and a wide angular range. *IEEE Trans. Antennas Propag.* **2017**, *65*, 4293–4298.
28. Liu C.-M.; Xiao S.; Zhang Z.; Feng J. Low profile SIW slot antenna with wide beam-width radiation pattern. *Electron. Lett.* **2018**, *54*, 116–118.
29. Yu C.A.; Li E.S.; Jin H.; Cao Y.; Su G.R.; Che W.; Chin K.S. 24 GHz Horizontally Polarized Automotive Antenna Arrays with Wide Fan Beam and High Gain. *IEEE Trans. Antennas Propag.* **2019**, *67*, 892–904.
30. Cheng Y.-F.; Ding X.; Shao W.; Yu M.-X.; Wang B.-Z. 2-D Planar Wide-Angle Scanning-Phased Array Based on Wide-Beam Elements. *IEEE Antennas Wirel. Propag. Lett.* **2017**, *16*, 876–879.
31. Su G.-R.; Li E.S.; Kuo T.-W.; Jin H.; Chiang Y.-C.; Chin K.-S. **79**-GHz Wide-Beam Microstrip Patch Antenna and Antenna Array for Millimeter-Wave Applications. *IEEE Access* **2020**, *8*, 200823–200833.
32. Lee, J.-H.; Lee, J.M.; Hwang, K.C. Sector-Beam Antennas for Wide Detection Area in 79 GHz Automotive Short Range Radar (SRR) Sensor. In Proceedings of the 2018 Asia-Pacific Microwave Conference (APMC), Kyoto, Japan, 6–9 November 2018; pp. 39–40.
33. Jinghu S.; Li H.; Yuanyuan Z.; Di Z. A 77GHz Millimeter Radar Flat-Shoulder Beam Array Antenna Design. In Proceedings of the 2021 IEEE International Workshop on Electromagnetics: Applications and Student Innovation Competition (iWEM), Guangzhou, China, 7–9 November 2021; pp. 1–3.
34. Nysaeter, A. Two-way MIMO Sparse Array Antenna Optimization with NSGA-III. In Proceedings of the 2020 IEEE Radar Conference (RadarConf20), Florence, Italy, 21–25 September 2020; pp. 1–6.
35. Hamza, A.; Qureshi, K.K.; Sheikh, S.I.; Attia, H. Linear and Planar Antenna Array Nulling based on Schelkunoff Polynomial and Genetic Algorithm. In *Proceedings of the* 2020 IEEE Radio and Wireless Symposium (RWS), San Antonio, TX, USA, 2–29 January 2020; pp. 112–115.
36. Yang, G.; Qin, Z.; Ji, Y.; Fang, G. W-Band MIMO Radar Array Optimization and Improved Back-projection Algorithm for Far-Field Imaging. In Proceedings of the 2019 44th International Conference on Infrared, Millimeter, and Terahertz Waves (IRMMW-THz), Paris, France, 1–6 September 2019; pp. 1–2.
37. He, X.; Alistarh, C.; Podilchak, S.K. Optimal MIMO Sparse Array Design Based on Simulated Annealing Particle Swarm Optimization. In Proceedings of the 2022 16th European Conference on Antennas and Propagation (EuCAP), Madrid, Spain, 27 March–1 April 2022; pp. 1–5.
38. Han Y.; Zhang D.; Huang C.; Jiang J.; Zhou L. A 60GHz Series-fed Microstrip Patch Antenna Array for Millimeter Wave Automotive Radar Application. In Proceedings of the 2024 Photonics & Electromagnetics Research Symposium (PIERS), Chengdu, China, 21–25 April 2024; pp. 1–7.
39. Heo J.M.; Kim K.; Choi J.; Byun G. Optically Transparent Series-Fed Microstrip Array with Small Inter-Element Spacing and Stepped Feed-Lines for Antenna-on-Display. *IEEE Access* **2024**, *12*, 99684–99692.
40. Song, H.; Fan, Q.; Wang, Y.; Li, Z. A Millimeter-Wave Wideband Patch Array Antenna with Parallel Connected Series-Fed Network. In Proceedings of the 2024 IEEE International Workshop on Antenna Technology (iWAT), Sendai, Japan, 15–18 April 2024; pp. 153–155.